Attitude Determination and Control System for University of Illinois Nanosatellite Architecture

Final Report

ECE 445 - Group 1

Rick Eason - reason2@illinois.edu
Srikar Nalamalapu - svn3@illinois.edu
Shamith Achanta - shamith2@illinois.edu

University of Illinois Urbana-Champaign - Electrical and Computer Engineering Department

May 4, 2022

Contents

1 Introduction

The University of Illinois Aerospace Engineering department's Laboratory for Advanced Space Systems at Illinois (LASSI) develops nanosatellites for the University of Illinois. Their next-generation satellite architecture is currently in development, however the core bus does not contain an Attitude Determination and Control (ADCS) system. An ADCS system is a spacecraft subsystem that is capable of performing controlled changes and determination of a spacecraft's attitude.

Our objective was to design an IlliniSat specification compliant ADCS module. This module should be capable of sensing the Earth's magnetic field, sensing the body rotation rate of the module, executing algorithms to generate control solutions, and actuate those solutions using magnetorquer coils.

A magnetorquer coil is a solenoid coil that can be commanded to generate a field of a certain strength and direction. This field interacts with Earth's magnetic field and generates a body torque on the spacecraft [1]. This form of solid-state attitude control is very weak, and as such is only used on small spacecraft.

In order for an ADCS system to be useful to LASSI, the system must be compliant with their modular spacecraft bus architecture. This module shall be physically, electrically, and digitally compliant with LASSI specifications. One of the important factors in the design of magnetorquer devices is the shape and size of the driving coils. The coils must be simultaneously efficient at producing a magnetic field, and be small enough to fit inside, but not waste space in, a nanosatellite bus. To that end, we have analyzed contemporary solutions, as well as studies of the optimization of magnetorquers [2], to develop driving coil geometries that are both compact and make efficient use of the current being fed through them.

2 Design

2.1 Design Procedure

2.1.1 Magnetic Coils and Constant-Current Drivers

Our magnetorquer system was designed to be both simple to manufacture as well as efficient. For our purposes efficiency is defined by the ratio of current through the coil and the coil maximum field strength. Current through the coil is determined by the coil series resistance. The maximum coil field strength is determined by equation 1, where l is the length of the solenoid, N is the number of turns in the coil, and I is the current through the coil.

$$\vec{B} = \mu_0 \frac{N \cdot I}{l} \tag{1}$$

We performed an analysis on several different constant-current architectures and determined that an op-amp current-feedback architecture was the best option for our purposes [3]. The constant-current drivers which drive current through the magnetorquer coils use a MOSFET to control the current through the device. The gate of this FET is driven by the output of a simple op-amp feedback circuit, which reads the difference between the voltage across a sense resistor and the voltage set by the microcontroller.

This system topology was chosen due to its simplicity and use of discrete parts. The use of discrete parts reduced our reliance on monolithic ICs, which are currently in short supply.

2.1.2 Sensing

The design of our sensing subsystem was driven by a need for valid data. In order to accurately determine a control solution, the geomagnetic field vector experienced by the spacecraft must be determined. The geomagnetic field is quite weak however, so the sensors must be sufficiently sensitive that they can accurately read the field. The same requirements apply to the gyroscopic sensors which determine the spacecraft body rotation rates.

According to the National Oceanic and Atmospheric Administration, the geomagnetic field strength ranges from between roughly 25 and 65 μT [4]. We used 25 μT as a conservative estimate for the magnetic field the system will encounter around the planet.

We need to accurately determine rotation rates that are very low, therefore we also selected a gyroscope that was sensitive to rates dramatically less than 1 degree per second.

Due to global IC shortages, we were limited in the fully-integrated sensing ICs that were available to us. As such, we elected to procure one IC for gyroscopic sensing, and one for magnetic sensing.

2.1.3 Processing and Interface

As part of our design requirement to maintain compatibility with LASSI standards, we are obligated to design our system using many of the same parts as are used in other spacecraft components. As such, components like the RS-422 transceiver, CAN bus transceiver, and stack interface connector were all selected because they are the same device used by other spacecraft modules.

This is also true for the microcontroller. The MCU we selected is the STM32L552, this is a very capable low-power device that contains many of the peripheral interfaces that we needed for the project. The device is capable of natively running an RTOS, which allows us to more easily modularize our firmware.

2.2 Design Detail

2.2.1 Magnetic Coils and Constant-Current Drivers

For each of our three solenoid coils, we wraped 1000 ± 3 windings of wire around the coil. Coils X and Y each have a mandrel diameter of 8mm and a length of 60mm, while coil Z has a mandrel diameter of 6mm and a length of 20mm to accommodate a reduction in vertical height for that coil. The Ohmic resistance of each coil is calculated from the geometric parameters and the resistivity of copper, $1.68 \times 10^{-8}\ \Omega \cdot m$. We are using 32 AWG enameled copper wire, which is 3.2×10^{-8} m^2 in cross-sectional area.

$$R = \frac{\rho \cdot L}{A} \tag{2}$$

Equation 2 shows the relationship between the resistance of a wire, the length L of the wire in meters, the cross-sectional area of the wire in m^2, and the resistivity ρ of the wire in Ohm-meters.

$$L = N \cdot C \cdot 1.005 = N \cdot 1.005 \cdot (2\pi \cdot r) \tag{3}$$

Equation 3 shows the computation of the length of the wire as being the product of the number of wire wrappings N, the circumference of the coil $(2\pi \cdot r)$ in meters, and a 0.5% fudge factor to account for imperfect windings.

We can combine equations 2 and 3:

$$R = \frac{1.005\rho N(2\pi r)}{A} \tag{4}$$

$$R_{X\&Y} = \frac{1.005\rho N(2\pi r)}{A} = \frac{1.005(1.68 \times 10^{-8})1000(2\pi(0.004))}{3.2 \times 10^{-8}} = 13.261\Omega \tag{5}$$

The series resistance of coils X and Y, as calculated in equation 5, should be roughly 13.62 Ohms. The resistance of the Z axis coil requires an adjustment. Due to the shorter nature of the coil, the wire must be wrapped over itself in a series of layers in order to reach the desired number of turns. This increases the radius of each layer of wire and thereby increases its length. The width of the 32 AWG wire is 0.202 mm. Dividing the length by this gives the number of turns per layer, and adding the wire thickness to each successive layer radius will account for the increased length.

$$T_l = \frac{20}{0.202} = 99.059 \tag{6}$$

With almost exactly 100 turns per layer, the coil will be almost exactly 10 layers deep.

$$\sum_{n=0}^{9} T_l * C_n = \sum_{n=0}^{9} 99 * ((0.003 + (n * 0.00202)) * 2 * \pi) \approx 25.25m \tag{7}$$

Where T_l is the turns per layer and D_n is the circumference of layer n. Using calculation 7 of 25.25 meters of wire, the coil resistance can now be calculated.

$$R_Z = \frac{1.005\rho L}{A} = \frac{1.005(1.68 \times 10^{-8})25.25}{3.2 \times 10^{-8}} = 13.602\Omega \tag{8}$$

With equations 5 and 8 we estimated that despite having different geometries, the coil resistances will be essentially the same.

From here an analysis of magnetic field strength was performed. We used the maximum current produced by the constant current drive in simulation as the drive current in this analysis, 175 mA. Equation 9 describes the related parameters of the B field created by the solenoid.

$$\vec{B} = \mu_0 \frac{N \cdot I}{l} \tag{9}$$

Where l is the length of the solenoid. For coils X and Y this is 60mm and for coil Z this is 20mm.

$$\vec{B}_{X\&YMAX} = \mu_0 \frac{1000(0.175)}{0.06} = 3.665mT \tag{10}$$

$$\vec{B}_{ZMAX} = \mu_0 \frac{1000(0.175)}{0.02} = 10.996mT \tag{11}$$

As shows in equations 10 and 11, our design should generate magnetic fields in the milli-Tesla range.

2.2.2 Sensing

Our device used the Rohm Semiconductor BM1422AGVM three-axis magnetometer as our magnetic field sensor. Table 1 is a comparison between the rated performance of the device and our required performance.

Table 1: Magnetometer Performance Requirements Comparison

Specification	**BM1422AGVM Rated Performance**	**Required Performance**
Measurable Magnetic Range:	$\pm$1200μT	$\pm$65μT
Magnetic Sensitivity:	0.042μT/LSB	0.1μT/LSB
Input Voltage Range:	1.7-3.6V	3.3V $\pm$0.1V
Operating Temperature Range:	-40 to +85°C	$\pm$40°C

Comparison between the rated performance of the device and our required performance.

As is shown by table 1, the BM1422AGVM meets or exceeds all relevant required parameters. In addition to this, the device contains a user-variable low-pass filter. Use of this filter will allow us to filter out high-frequency noise without consuming MCU processing time to do so.

For sensing gyroscopic rotation we selected a Bosch Sensortech BMI270 three-axis gyroscope. Table 2 is a comparison between the rated performance of the device and our required performance.

Table 2: Gyroscope Performance Requirements Comparison

Specification	**BMI270 Rated Performance**	**Required Performance**
Measurable Rotation Rate Range:	$\pm$2000 dps	$\pm$50 dps
Rate Sensitivity:	16.384 LSB/dps	10 LSB/dps
Input Voltage Range:	1.7-3.6V	3.3V $\pm$0.1V
Operating Temperature Range:	-40 to +85°C	$\pm$40°C

Comparison between the rated performance of the device and our required performance.

As shown in table 2, the BMI270 meets or exceeds all relevant required parameters.

2.2.3 Processing and Interface

The interface design of our device was determined primarily by the requirement that our device be physically and electrically compatible with LASSI's IlliniSat hardware standards. This prescribed the physical dimensions of the

board, as well as the placement and selection of the stack connector. Figure 1 shows a final render of the board as it was ordered.

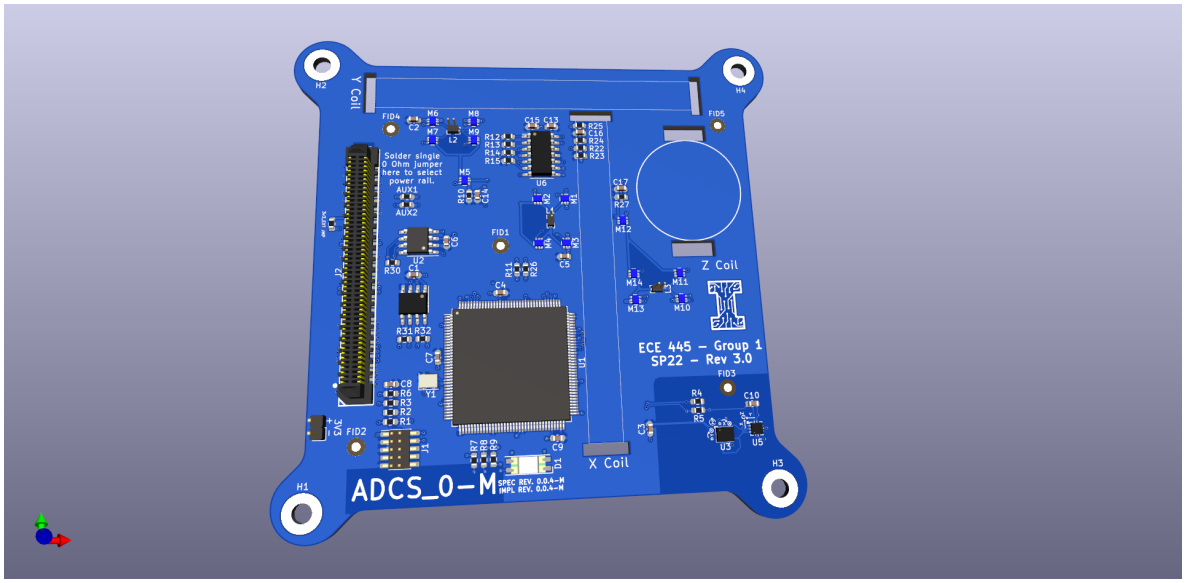

Figure 1: Final render of the board as ordered.

The shape of the board is deliberate as when many boards of the same outline are stacked together the edges inset from the sides form cable trenches, which allow components not connected to the main stack connector to interconnect with cable harnesses. The pinout of the stack connector and which serial and power interfaces our device connects to are also prescribed by LASSI standards.

Our PCB is four layers, and we optimized the layout to maximize contiguous flood planes on the top and bottom. This shields the serial and analog data lines that traverse the board and reduces the amount of noise which is coupled into them. Cutout notches are also included where the feet of the coil mandrels are clipped into the board. An image of the layout of our PCB is shown in figure 2.

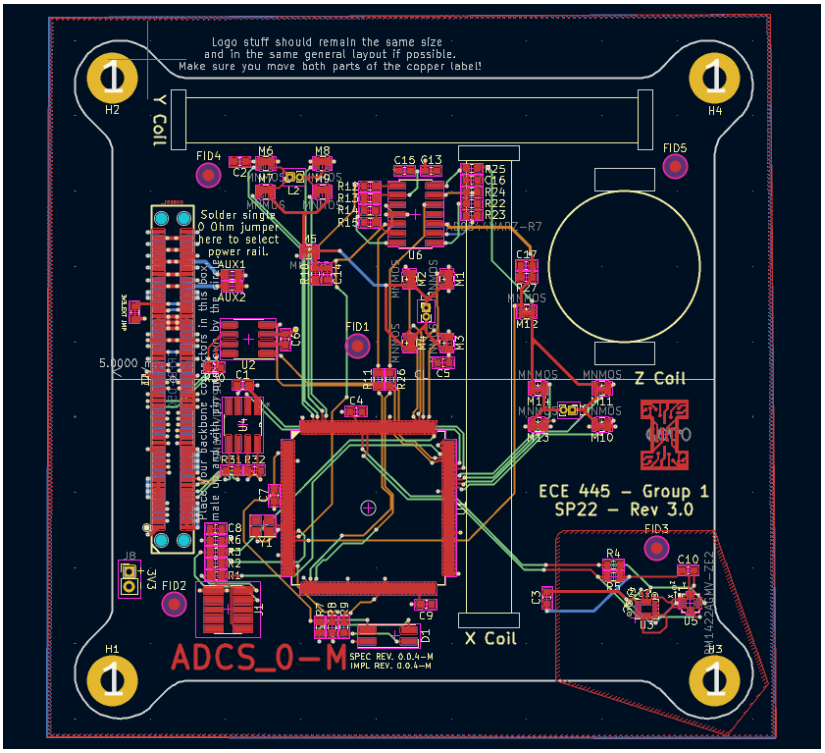

Figure 2: Layout of PCB. Red indicates top layer copper, Green is layer 2, Orange is layer 3, and Blue is the bottom layer copper.

Our microcontroller must be able to execute commands and run its peripherals extremely fast in order to complete all the required tasks without running out of time. As such, our MCU core clock is 105 MHz. This allows us to super-sample all of our input peripherals, as well as complete mathematics tasks thousands of times faster than the sensor data changes. This provides us significant headroom for the time consuming matrix operations which ADCS solution algorithms require.

3 Verification

3.1 Magnetic Coils and Constant-Current Drivers

The testing and verification process for the magnetic coils was straightforward. First, a multimeter was used to measure the resistance of each coil at the solder joints to the PCB. Under most circumstances it is not possible to measure the resistance of one component while it is in-circuit. However, because the coils are inside an H-bridge, the coil is effectively isolated from the rest of the circuit while the bridge is in the off state. Table 3 shows the resistances of the coils as measured.

Table 3: Measured Coil Resistance

Coil	**Resistance [Ω]**
X	15.32
Y	15.96
Z	18.54

The Ohmic resistance of each coil as measured by a multimeter.

Testing firmware was written to put the coils into maximum current level and set the H-bridges to their forward setting. A magnetometer was placed at the aperture of each coil and the difference between the measured field and the background field was measured. Table 4 shows the measured fields for each coil, as well as the magnitude of the deviation from the predicted field strength.

Table 4: Measured Coil Maximum Field

Coil	**Field Strength [mT]**	**Deviation From Estimate [mT]**
X	3.424	0.241
Y	3.303	0.362
Z	10.039	0.957

The maximum magnetic field strength per coil measured at the coil aperture. The deviation is determined by the difference between the recorded value and the value estimated by equations 10 and 11.

We believe that the consistent under-estimation of the coil resistance, and therefore the slight under-performance of the magnetic field generation, is due to imperfect coil winding. Imperfections in the coil winding cause a small but cumulative increase in the length of the wire, which has a macroscopic effect after 1000 windings.

According to our requirements, success is declared if our generated fields are within one order of magnitude of our estimated fields. Given that this is the case, we conclude that the constant-current drivers and the magnetorquer coils are have been successfully implemented.

3.2 Sensing

The sensing subsystem proved more difficult to test due to our lack of access to precision test hardware for magnetic field creation and rotation rates. We developed a basic testing methodology for the magnetometer in which we compared the data it read out to data determined by a smartphone magnetometer nearby. The resulting values and deviations have been recorded in table 5.

Table 5: Magnetometer Verification

Sensor Axis	BMI270 Field Strength [μT]	Smartphone Field Strength [μT]	Deviation [μT]
X	5.26	5.40	0.14
Y	4.41	4.23	-0.18
Z	-45.20	-44.91	0.29

Comparison of data recorded by BMI270 sensor on our device and a comparable magnetometer in a smartphone.

As shown in table 5, the BMI270 sensor in our device records accurate data that is well bellow 1 micro Tesla in deviation. This exceeds our criteria for success and we determine that this sensor has been implemented successfully.

Testing of the gyroscopic sensor is difficult without a complex mechanism to support rotations in 3d space. As such we tested our sensor on an un-moving flat surface to determine sensor drift over a period of one hour of operation. The results of this test are recorded in table 6.

Table 6: Gyroscope Verification

Sensor Axis	Initial Measurement [dps]	Final Measurement [dps]	Deviation [dps]
X	0.0000	0.0001	0.0001
Y	0.0000	-0.0002	-0.0002
Z	0.0001	0.0002	0.0001

Results of one hour zero-rate drift test of gyroscope data.

As shown in table 6, the gyroscope reading remains highly accurate over a long period of time. This is considered a success by our validation criteria.

3.3 Processing and Interface

The processing requirements for our system are met by a combination of factors. These include both the nameplate performance of the STM32L552 microcontroller, as well as a qualitative analysis by our team.

With a core clock of 105 MHz, a hardware floating-point unit, and a all serial, PWM, and GPIO interaction handled by hardware peripherals, the STM32L552 is sufficiently performant to meet our requirements. During our resting our team did not encounter any situation or condition which met or exceeded the processor's maximum operation speed. At no time did we run out of memory or have to wait for an operation to complete for longer than is normal.

These factors allow us to conclude that the STM32L552 microcontroller, and the CMSIS v2 RTOS layer on top of it, meet our requirements for the processing subsystem.

The interface requirements for our device fall into two categories; mechanical, electrical, and digital. We meet our requirements for mechanical interfacing by using the LASSI IlliniSat standard board layout to design our board. We further comply with that requirement by using the LASSI IlliniSat standard placement and footprints for the stack interface connector.

We meet our requirements for electrical interfacing with our adherence to the LASSI IlliniSat standard stack connector pinout. Per our routing, we passthrough all conductors in the stack connector, which is required by IlliniSat standards. In order to validate our requirements on current limits, we configured our device to operate at maximum output, with all three coils running at maximum level and both sensors collecting data at a high rate. We measured the

current being supplied to the device and found that it consumed only 932 mA at the 3.3V it was supplied with. This is well bellow our limit of 2 amps.

We were unfortunately unable to test serial interfacing through the stack connector over RS-422 and CAN bus. This was due to a combination of insufficient time, as well as a lack of access to a taller variant of the stack connector we used. Due to the height of the solenoid coils, the connector is too short to interface with our stack test board. However, due to the nature of RS-422 and CAN transceivers, we are very confident that those devices would work if we had the time to test them.

4 Costs

4.1 Labor

The hourly wage for a research project is estimated to be $18 an hour, and our total time commitment was 15 hours/week for 12 weeks. We estimate a labor cost of $8100 per person. Therefore, the total labor cost is estimated to be $24,300. This is broken out in table 7.

Table 7: Labor Cost Analysis

Name	**Weekly Hours**	**Hourly Pay**	**Fudge Factor**	**Weeks**	**Cost (USD)**
Rick	15	18	2.5	12	8,100.00
Srikar	15	18	2.5	12	8,100.00
Shamith	15	18	2.5	12	8,100.00
Total:					**$24,300.00**

Per-person breakdown of labor costs for the project.

4.2 Parts

The cost of parts for this project is significant. Due to shortages in global semiconductor supply, the cost of many parts of the system have increased dramatically. Table 8 is a list of all parts purchased. This list does not include the cost of shipping.

Table 8: Itemization of Parts Purchased

Part Name or Number	**Quantity**	**Cost (USD)**
AD8544WARZ Quad Op-Amp	10	22.19
ERM8-050 Stack Connector	1	11.01
ERF8-050 Stack Connector	1	10.38
SSM6k211FE NFET	30	13.80
RGB LED	10	2.40
32 AWG Copper Wire Spool	1	10.85
SN65HVD232 CAN XCVR	3	9.75
SN65HVD379 RS-422 XCVR	6	40.68
BMI270 IMU	4	59.96
BM1422AGMV IMU	10	66.10
STM32L552 MCU	2	25.08
JTAG and 1.27mm Pin Headers	5	10.00
90x90mm 4-layer HASL main PCB	5	75.00
20x20mm 2-layer ENIG MCU carrier PCB with μVias-in-pad	5	66.00
ST Nucleo STM32L552 Devkits	*3*	*63.84*
19.2 MHz XO	*10*	*6.42*
Subtotal		*70.26*
Subtotal		463.20
Total		**$533.46**

List and summation of cost of parts purchased. Item listed in *italics* were purchased out of the ECE department-provided budget, all else was purchased by the group.

4.3 Total Cost

Table 9: Total Cost

Category	**Cost (USD)**
Labor	24,300.00
Requisitioned Parts	*533.46*
Total	**$24,833.46**

This is a summation of the total costs we project to see for this project. Real costs, ones that involve actual purchasing, are marked in *italics*. Labor costs, which are a fabrication for this project as in fact we are paying to take this class, are in standard type.

5 Conclusion

While this project does not pose any significant ethical concerns on its own, and by its nature is incapable of doing anything on its own, it is designed for use on a spacecraft. Spacecraft development is not an ethically negligible engineering field. Prior to 2013, the United States federal government classified technology such as this project as "munitions" and restricted export of it and access to materials pertaining to it to U.S. citizens and green card holders only. Since then the related laws, the International Traffic in Arms Restrictions (ITAR), have been adjusted to remove this form of satellite technology from the list of munitions technology. [5]

Whenever an object is launched into orbit, two primary ethical questions are raised. How long will it take to come back down, and will it hit anything when it does? NASA guidelines require all cubesat-class satellites to re-enter the atmosphere within 10 years of launch, which is a very short lifetime for orbital debris. This requirement is enforced outside the scope of this project, and is therefore not relevant. Secondly, orbital debris can sometimes survive interfacing with the atmosphere on re-entry. This occurs to spacecraft components as a function of their orbital energy, material, and geometry. The U.S. FCC is the authority on restricting falling debris, they require the formulation of an Orbital Debris Assessment Report (ODAR) in order to grant a license to a satellite for the use of radio spectrum for communications. In order to abide by this standard, we did not use materials which commonly survive re-entry.

The initial impetus for this project concept was to use ECE 445 to prototype the development of an ADCS unit for LASSI. To that end, this project has been incredibly successful. Even though problems occurred, and the project has limited visual flair, the overall goal has been achieved. Critical lessons learned have been encountered and understood, and practical suggestions for future work on this or a similar device have been generated. We have accomplished much in this semester; design of a variable set-point constant-current driver, design of a device into pre-defined interface requirements, successful implementation of an RTOS in an embedded microcontroller environment, and implementation of serial peripheral devices in an embedded device.

The eventual goal for LASSI's development of the next-generation IlliniSat program is to put spacecraft into the hands of middle school and high school students. This is a monumental task which required having a highly modular spacecraft bus architecture, inexpensive components, and wide tolerances for performance. If this program is successful, every K12 STEM student in the state of Illinois will have had their hands on hardware that is in orbit around the planet. The work our team has done for this project is just a small part of that idea, and we are incredibly proud of the work we have done.

References

[1] P. Wang, Y. Shtessel, and Y.-Q. Wang, "Satellite attitude control using only magnetorquers," in *Proceedings of Thirtieth Southeastern Symposium on System Theory*, 1998, pp. 500–504. DOI: 10.1109/SSST.1998.660124.

[2] I. Indir, K. Sever, I. Vnučec, and J. Lončar, "Design and optimization of air core magnetorquers for attitude control of leo nanosatellites," in *2021 International Symposium ELMAR*, 2021, pp. 135–138. DOI: 10.1109/ELMAR52657.2021.9550888.

[3] R. Stephens, "White paper: Expanding the usability of current-feedback amplifiers," Texas Instruments Incorporated, Dallas, Texas, Tech. Rep. SLYT099, Q3 2003, p. 7. [Online]. Available: https://www.ti.com/lit/an/slyt099/slyt099.pdf?ts=1644437138816.

[4] A. S. M. P. A. C. B. M. N. B. H. A. W. V. R. S. M. A. T. N. G. M. T. Chulliat, "The us/uk world magnetic model for 2015-2020," National Geophysical Data Center, NOAA, Jan. 2015, p. 112. [Online]. Available: https://www.ngdc.noaa.gov/geomag/WMM/data/WMM2015/WMM2015_Report.pdf.

[5] P. Marks. "US no longer lists satellites as weapons." (), [Online]. Available: https://www.newscientist.com/article/dn23058-us-no-longer-lists-satellites-as-weapons/.